UC Davis
San Francisco Estuary and Watershed Science

Title
Flow Convergence Caused by a Salinity Minimum in a Tidal Channel

Permalink
https://escholarship.org/uc/item/2m6367vc

Journal
San Francisco Estuary and Watershed Science, 4(3)

Authors
Warner, John C.
Schoellhamer, David H.
Burau, Jon R.
et al.

Publication Date
2006

DOI
10.15447/sfews.2006v4iss3art1

Copyright Information

Peer reviewed

Flow Convergence Caused by a Salinity Minimum in a Tidal Channel

John C. Warner*
David H. Schoellhamer
Jon R. Burau
U.S. Geological Survey, Placer Hall, 6000 J Street, Sacramento, CA, 95819

S. Geoffrey Schladow
University of California, Davis

*****Corresponding author:** Jcwarner@usgs.gov

ABSTRACT

Residence times of dissolved substances and sedimentation rates in tidal channels are affected by residual (tidally averaged) circulation patterns. One influence on these circulation patterns is the longitudinal density gradient. In most estuaries the longitudinal density gradient typically maintains a constant direction. However, a junction of tidal channels can create a local reversal (change in sign) of the density gradient. This can occur due to a difference in the phase of tidal currents in each channel. In San Francisco Bay, the phasing of the currents at the junction of Mare Island Strait and Carquinez Strait produces a local salinity minimum in Mare Island Strait. At the location of a local salinity minimum the longitudinal density gradient reverses direction. This paper presents four numerical models that were used to investigate the circulation caused by the salinity minimum: (1) A simple one-dimensional (1D) finite difference model demonstrates that a local salinity minimum is advected into Mare Island Strait from the junction with Carquinez Strait during flood tide. (2) A three-dimensional (3D) hydrodynamic finite element model is used to compute the tidally averaged circulation in a channel that contains a salinity minimum (a change in the sign of the longitudinal density gradient) and compares that to a channel that contains a longitudinal density gradient in a constant direction. The tidally averaged circulation produced by the salinity minimum is characterized by converging flow at the bed and diverging flow at the surface, whereas the circulation produced by the constant direction gradient is characterized by converging flow at the bed and downstream surface currents. These velocity fields are used to drive both a particle tracking and a sediment transport model. (3) A particle tracking model demonstrates a 30 percent increase in the residence time of neutrally buoyant particles transported through the salinity minimum, as compared to transport through a constant direction density gradient. (4) A sediment transport model demonstrates increased deposition at the near-bed null point of the salinity minimum, as compared to the constant direction gradient null point. These results are corroborated by historically noted large sedimentation rates and a local maximum of selenium accumulation in clams at the null point in Mare Island Strait.

KEYWORDS

SUGGESTED CITATION

INTRODUCTION

The transport and residence times of dissolved constituents and suspended sediment in estuarine waters are influenced by residual (tidally averaged) circulation patterns. These circulation patterns are controlled by such factors as tidal currents interacting with the geometry, bathymetry, wind, geophysical rotation, freshwater inflow, and the balance between barotropic (water surface) and baroclinic (density) pressure gradients. The focus of this paper is on the effect of the longitudinal density structure (magnitude and direction) on residual circulation patterns.

A typical estuary has a longitudinal density gradient in a constant direction corresponding to higher density water at the mouth and lower density water at the head. Changes in the magnitude of the gradient along the length of the estuary can create regions of convergence or divergence of the tidally averaged flow field and lead to zones of either enhanced sediment deposition or erosion, respectively. Hansen and Rattray (1965) describe classical, two-layer, estuarine circulation and the development of a convergent null zone. The null zone occurs where the pressure forces at the estuary bottom resulting from the longitudinal density and water surface gradients are in balance. More recently Largier, et al. (1996) discuss circulation patterns that evolve from spatially changing density structures in low-inflow estuaries; Wolanski (1988) describes circulation due to a salinity maximum region created by evaporation that drives a diverging near-bed flow pattern and converging surface current; and Jay and Musiak (1994) and Burau, et al. (1998) discuss
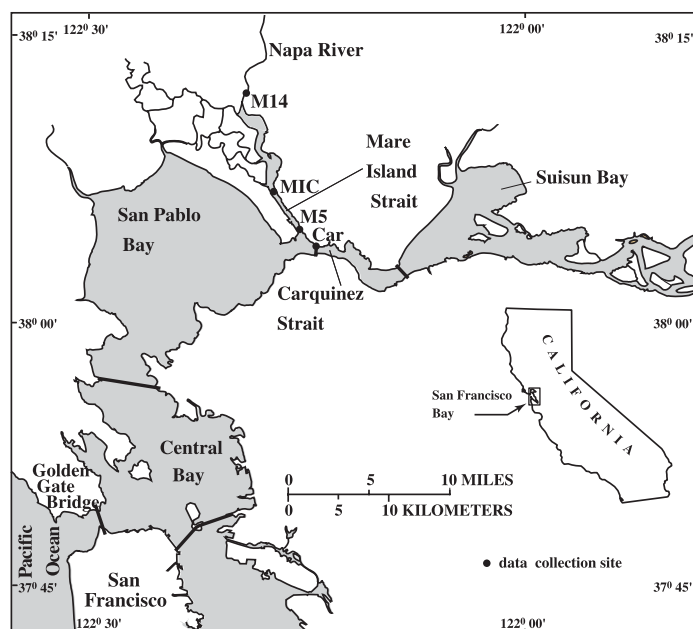
Figure 1. Site map of San Francisco Bay, California.

bathymetric control on density gradients and residual circulation.

Here we show that differential tidal phasing near channel junctions can affect the magnitude and direction of the longitudinal density gradient. Warner, et al. (2002) report that a local salinity (density) minimum develops due to the tidal current phasing and salt transport that occurs at the junction of two tidal channels, Mare Island Strait and Carquinez Strait, in northern San Francisco Bay, California. The local salinity minimum develops in Mare Island Strait (Figure 1). The tidal characteristics of Mare Island Strait resemble a standing wave (water level and horizontal velocity are 90 degrees out of phase), and those in Carquinez Strait are more progressive (water level and horizontal velocity are in phase), creating a difference in tidal current phase between the two straits. The tidal currents in Mare Island lead those in Carquinez and, therefore, the currents in Mare Island Strait will begin to flood first and receive a decreasing salinity while Carquinez Strait is completing its ebb. Then, Mare Island Strait receives an increasing salinity when Carquinez Strait floods. This tidal phase difference creates the local salinity minimum in Mare Island Strait during each tidal cycle. Because the tidal prism in Mare Island Strait is less than one-tenth the size of

that in Carquinez Strait, the phasing effect produces a pronounced salinity minimum in Mare Island Strait, but has minor influence on salinity in Carquinez Strait.

In this paper simulations using a 1D advection-dispersion equation for salinity demonstrate that differences in tidal current phasing at the junction of two straits can create a local salinity minimum. A 3D model is used to investigate the vertical structure of tidally averaged circulation in the vicinity of a local salinity minimum and to compare it with the circulation when the salinity gradient is in one direction only. It is shown that in the presence of a local salinity minimum, the vertical circulation is caused by opposing longitudinal gradients in density that meet at the location of the minimum. In this case of no salinity minimum, the gradient of density is in one direction and vertical circulation is in the form of classical estuarine circulation. Particle tracking and sediment transport models are used to show that a tidal channel having a salinity minimum has increased residence times of neutrally buoyant particles and increased sediment deposition rates (respectively) when compared to a tidal channel having a density gradient in one direction.

METHODS

Data Collection

Data were collected from September 1997 to March 1998 at three sites along the Napa River and at one site in Carquinez Strait (Figure 1): channel marker 14 (M14, river km 18), Mare Island Causeway (MIC, river km 7), channel marker 5 (M5, river km 2), and Carquinez (Car). Acoustic Doppler current profilers (ADCPs) provided mean velocity measurements every 20 minutes at all sites except Car. Conductivity, temperature, and water level were measured at all sites on taut-wire moorings with above-bed sensor heights of 1 m at M14, 1 m and 7 m at MIC, 1 m and 6 m at M5, and 1 m and 20 m at Car at 15 minute intervals (Warner et al., 1999). Fresh water inflow into Mare Island Strait from the Napa River was relatively minor during this period and was neglected.

Numerical Models

Four types of numerical simulations were used in this study: (1) a 1D finite difference model to demonstrate the formation of a local salinity minimum in Mare Island Strait, (2) a 3D finite element model to compare the tidally averaged current structure from a salinity minimum to a constant direction gradient, (3) a particle tracking model to quantify residence times, and (4) a sediment transport model to reveal the increased deposition rates associated with the circulation caused by the salinity minimum circulation.

1D finite difference semi-analytical model (development of salinity minimum)

To demonstrate the formation of a local salinity minimum by tidal current phase differences, a finite difference model was used to solve the 1D advection-dispersion equation for salinity in Mare Island Strait. The model is based on an analytical solution for the velocity field and an explicit numerical solution of the salt transport equation. The velocity was modeled according to a linearized form of the 1D continuity and momentum equations (Ippen, 1966)

$$\frac{\partial \eta}{\partial t} = -h \frac{\partial \overline{v}}{\partial y} \tag{1}$$

$$\frac{\partial \overline{v}}{\partial t} = -g \frac{\partial \eta}{\partial y} - M \overline{v} \tag{2}$$

where:

$$M = \frac{8}{3} \frac{C_f}{\pi} \frac{V_0}{h} \tag{3}$$

and η is the vertical change of the water surface from the undisturbed level, h is the mean channel depth, $\overline{v}$ is the cross-sectionally averaged velocity, y is the longitudinal coordinate (y = 0 at the mouth and y = 30 km at the upstream terminous), t is time, g is acceleration of gravity, M is the linearized friction term, C_f is the friction coefficient, and V_0 is the magnitude of the depth-averaged velocity. Because the tide in Mare Island Strait is representative of a standing wave (Warner, 2000), solutions for a channel closed at the upstream terminous (y = 30 km) were used.

$$\eta = A \left[e^{-\mu y} \cos(\sigma t - k y) + e^{\mu y} \cos(\sigma t + k y) \right] \tag{4}$$

$$\overline{v} = A \frac{c_0}{h} \frac{k_0}{\sqrt{\mu^2 + k^2}} \left[e^{-\mu y} \cos(\sigma t - k\,y + \alpha) - e^{\mu y} \cos(\sigma t + k\,y + \alpha) \right]$$

(5)

$$A = \frac{\eta_{lH}}{\sqrt{2(\cos(2k\,l) + \cosh(2\mu l))}}$$

(6)

$$\tan\alpha = \frac{\mu}{k}; \qquad \tan 2\alpha = \frac{M}{\sigma}$$

(7)

and $c_0 = \omega / k_0 = \sqrt{gh}$, $k_0 = 2\pi/L$, $\omega = 2\pi/T$, $k_0^2 = k^2 - \mu^2$, η_{lH} = maximum amplitude of high water at y = l (open end of the channel) and is obtained from observations, T = tidal period, and L = tidal wave length. Frictional damping affects these solutions by increasing the effective wave number from the undamped value k_0 and thus creates a shorter wavelength and slower propagation speed. Friction modifies the phase of the velocity by the parameter α and this shifts the timing of the maximum current relative to high water.

Equation 5 was used to construct the total spring/neap velocity variations ($\overline{v}_{total}$) in Mare Island Strait by separately calculating the contributions from the two principal tide-producing constituents, M2 (lunar) and S2 (solar), and then summing the results. The parameters μ and k were determined for the M2 and the S2 constituents using harmonic analysis of measured water-level time series at sites M14, MIC, and M5. The results were $\mu = 1.82 \times 10^{-6}$ and $k = 1.88 \times 10^{-5}$ for the M2, and $\mu = 6.23 \times 10^{-6}$ and $k = 1.28 \times 10^{-5}$ for the S2 (units of rad/m for both μ and k) (Warner, 2000). The analytical solution of the velocity in Mare Island Strait ($\overline{v}_{total}$) and the along-channel depth-average of the velocity measurements from site MIC compare well (Figure 2).

The analytical velocity was used in the numerical solution of the advection-dispersion equation

$$\frac{\partial s}{\partial t} + \overline{v}_{total} \frac{\partial s}{\partial y} = D_y \frac{\partial^2 s}{\partial y^2}$$
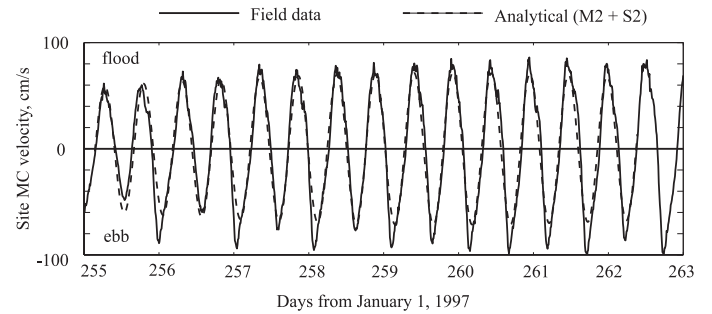
(8)

Figure 2. Time series of velocity at site MIC comparing depth-averaged field data (all constituents) to analytical model (M2 + S2).

that is discretized with an explicit forward-time, centered-space scheme as

$$s_m^{n+1} = s_m^n - \frac{\overline{v}_{total}\,\Delta t}{2\,\Delta y}\left(s_{m+1}^n - s_{m-1}^n\right) + \frac{D_y\,\Delta t}{\Delta y^2}\left(s_{m+1}^n - 2s_m^n + s_{m-1}^n\right)$$

(9)

where s is the magnitude of salinity, m is the spatial node number (m=y/Δy), n is the temporal step number (n=t/Δt), D_y is a 1D dispersion coefficient set to equal 10 m^{2}s^{-1} (results were not qualitatively sensitive to this value), and is calculated from equation 5. The grid was generated as a straight line 30 km in length to represent the Napa River, with an open boundary at the junction (y = 0 km) with Carquinez Strait and a closed boundary at the tidal limit (y = 30). The model was run with Δy = 50 m and Δt = 30 seconds. An initial condition of salinity s = 18.5 was established throughout the domain, and salinity boundaries were a zero gradient (no flux) condition at the tidal limit and measured time series salinity from site Car at the open boundary.

3D finite element model (residual current structure)
To characterize the residual current structure in the y-z plane resulting from the salinity minimum, a 3D finite element model, RMA-10, was applied to solve the coupled velocity and density field from the set of Reynolds averaged momentum equations, the continuity equation, the equation of state, and the advection-dispersion equation (King, 1996; Cook, 2000).

Two cases were modeled. The first is the case observed in Mare Island Strait in which a local salinity mini-
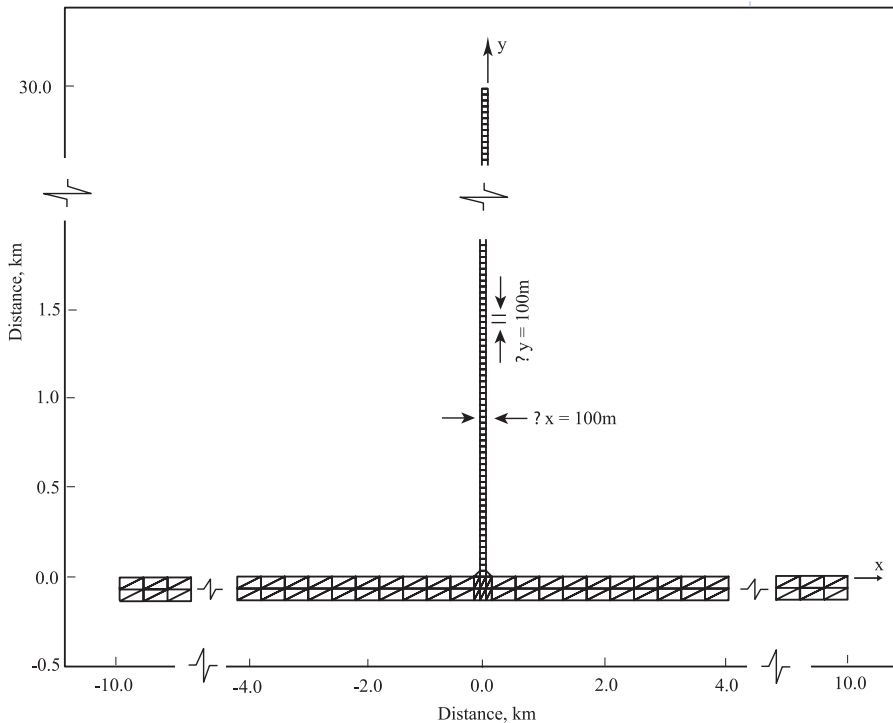
94

Figure 3. Domain for 3D hydrodynamic finite element model.

eddy diffusivity coefficients were solved for in the model by using the level 2.0 closure scheme described by Mellor and Yamada (1982) and then corrected for stability with the method of Henderson-Sellers (1982). Bed frictional resistance was parameterized using a Manning n value of 0.020.

The initial upstream boundary condition at y = 30 km was established as a typical, low dry-season freshwater flow of 1 m^3s^{-1}. A relatively weak longitudinal salinity gradient of -0.05 km^{-1} was established along the y-axis channel to simulate observed spring tide, slack-after-ebb conditions (Warner, 2000). Observations in Mare Island Strait show that the longitudinal salinity gradient at slack-after-flood tide is greater than at slack-after-ebb tide, indicating a contraction of the salt field during the flood and expansion during the ebb. This process was also observed by Burau et al. (1998) in Suisun Bay. The contraction is due to the greater velocities and hence greater change in salinity at the mouth (site M5) than near the head (site M14). With a distance of 30 km, this represented a salinity change of 1.5 along the length of the river from an initial value of 16.0 at y = 30 km to 17.5 at y = 0 km.

A typical San Francisco Bay longitudinal salinity gradient of -0.50 km^{-1} (Burau, et al., 1998) was established along the x-axis channel and allowed to oscillate across the mouth of the y-axis channel by varying the water surface elevations at x = -10 km and x = 10 km according to η=A cos(ωt + φ), where η is the water level (meters) relative to mean sea level, ω is the tidal period set at 12.0 hours (to represent a semi-diurnal tide), t is the cumulative time incremented in 10-minute steps, and φ is a phase parameter. To represent the observed case of the salinity minimum, the parameters at the left and right boundaries were A_{left} = 1.20 m and ϕ_{left} = 0° and A_{right} = 1.00 m and ϕ_{right} = 20°, which established a progressive wave in the x-axis channel. For the hypothetical case to establish a longitudinal density gradient with a constant direction along the y-axis channel, the parameters for the left and right boundaries were A_{left} = 1.00 m and ϕ_{left} = 0° and A_{right} = 1.25 m and ϕ_{right} = 20°,

mum exists. The second is a hypothetical case in which no current phase lag is assumed between the straits and thus creates a salinity gradient that continuously decreases landward (constant direction). Comparison between these two simulations will emphasize the difference in the resulting tidally averaged circulation patterns. The model geometry was chosen as a junction of two straight channels (Figure 3). The x-axis channel is 20 km long, 400 m wide, 11 m deep, and discretized with triangular elements. The channel of interest along the y-axis is 100 m wide and slopes from a depth of 11 m at the junction to 5 m at the head (a bottom slope of $2x10^{-4}$ m/m to approximate slope of Napa River). Longitudinal rectangular elements of 100 m in length were used to discretize the 30 km y-axis. In the vertical a boundary-fitted (sigma coordinate) grid was used with 10 layers.

The horizontal eddy viscosity and eddy diffusivity terms were assumed constant at 50 and 20 m^2s^{-1}, respectively for model stability. For San Francisco Bay, a typical value for both of these parameters is 10 m^2s^{-1} (Smith, 1997), which is similar in magnitude to the selected coefficients. The vertical eddy viscosity and

which established a standing wave in the x-axis channel. For both simulations the y-axis channel was a standing wave, and this created a 1.5-hour phase difference between the channels for the simulation of a salinity minimum and a 0.0-hour phase difference for the simulation of the constant direction gradient simulation. For each simulation the model was run until an initial dynamic solution was obtained using at least four tidal cycles to allow for "spin-up." This allowed time for the flow fields to develop in response to the pressure gradients.

Particle Tracking Module (residence time)

Results from both of the 3D hydrodynamic simulations were used to model transport of neutrally buoyant particles. The position of each particle is evaluated using a random walk model governed by the Ito stochastic differential equation (Dimou and Adams, 1993)

$$dx = x(t+dt) - x(t) = A(x(t),t)dt + B(x(t),t)dW(t)$$

(10)

where x is a two dimensional vector (y, z), A(x(t),t) is a known tensor representing the deterministic movement and B(x(t),t) is a stochastic component representing the random fluctuations of the particle movement, and dW(t) is the random Wiener process shown to have the properties of <dW> = 0 (zero time mean) and <dW dW> I dt (mean square proportional to dt), and I = identity matrix. As shown by Dimou and Adams (1993), the discretized form of equation 10, when taking the number of particles to Inf and the time step dt to 0, is equivalent to the advection dispersion equation written as

$$\frac{\partial c}{\partial t} + \frac{\partial}{\partial y}\left[vc + c\frac{\partial D_y}{\partial y}\right] + \frac{\partial}{\partial z}\left[wc + c\frac{\partial D_z}{\partial z}\right] = \frac{\partial^2}{\partial y^2}(D_y c) + \frac{\partial^2}{\partial z^2}(D_z c)$$

(11)

when

$$A = \left[v + \frac{\partial D_y}{\partial y}, w + \frac{\partial D_z}{\partial z}\right] \quad ; \quad \frac{1}{2}BB^T = \begin{bmatrix} D_y & 0 \\ 0 & D_z \end{bmatrix}$$

(12)

which leads to the particle transport formulation

$$y(t+dt) = y(t) + \left(v(t) + \frac{\partial D_y(t)}{\partial y}\right)dt + \sqrt{6 D_y(t) dt}\, R_2(t)$$

(13)

$$z(t+dt) = z(t) + \left(w(t) + \frac{\partial D_z(t)}{\partial z}\right)dt + \sqrt{6 D_z(t) dt}\, R_3(t)$$

deterministic   stochastic   (14)

where R_i (i = 2,3) is a vector of two independent uniform random numbers within the interval (-1, 1) (Dunsbergen and Stelling, 1993). To calculate the deterministic particle displacements, the hydrodynamic model results provide the velocity magnitudes of v and w. Because the horizontal eddy diffusivity (D_y) was held constant, the displacement calculated from the term for the spatial variation of the horizontal eddy diffusivity coefficient will be zero. Additionally, the hydrodynamic model was formulated using a free slip boundary on the sides (not the bottom) and uniform in the cross channel direction and thus does not model the effects on longitudinal dispersion due to lateral mixing. Therefore to include the effects of horizontal diffusivity in the particle tracking model, a 1D longitudinal dispersion coefficient (Fischer 1979, p.235) was calculated using

$$D_y = I_F \overline{v'^2} T_c f(T')$$

(15)

using $I_F = 0.01$ and $\overline{v'^2} = 0.05 \overline{v^2}$ (Bogle, 1997), $T_c = W^2/\varepsilon_t$, W is width = 100 m, ε_t is the transverse eddy diffusivity = 0.06 h $\overline{v}$, h is the average depth = 8 m, and f (T') is a function of the mixing time scale set to be 0.7 leads to (m^{2}s^{-1}). The vertical diffusivity D_z was calculated in the hydrodynamic model as discussed previously.

The tracking algorithm followed that by Pollock (1994) and Dunsbergen and Stelling (1993). To ensure mass conservation for the advection step, the path of each particle within a computational grid cell is described by the solution of the streamline equation

$$v_i^{ext}(\mathbf{x}, t) = \left(\frac{\partial \mathbf{u}}{\partial \mathbf{x}}\right)_{num} \Delta \mathbf{x}_{num} + \left(\mathbf{u}\big|_{x_p}\right)_{num} = \mathbf{a}_i \mathbf{x}_i + \mathbf{b}_i$$

(16)

where the subscript i is for each particle, v^{ext} is the velocity field used to translate each particle, $(\ )_{num}$ corresponds to the results from the numerical hydrodynamic model, and x_p is the location of each particle. Generalized to one dimension, the solution to equation (16) is of the form

$$T_p = \frac{1}{a} \ln \frac{X+C}{x_p + C}$$

(17)

where T_p is the time for a particle to reach the boundary of the computational cell, x_p is the original particle position within the computational cell, C = b/a, and X is the coordinate at either the right or left side of the computational cell, depending on relations between C and a, as described in detail by Dunsbergen and Stelling (1993).

At the beginning of each time step the location of each particle within a computational grid cell was identified. Then, the time required for each particle to reach the grid cell boundary was calculated using equation (17). Each particle was moved to the next cell boundary as long as the elapsed time was less than the hydrodynamic time step (600 seconds). The final particle displacement was computed as X from equation (17) with T_p substituted as the remaining time. This particle displacement procedure ensures that the particles will not cross a cell boundary where the normal velocity component is zero. Displacements due to the stochastic components then were added. Particles that were transported vertically out of the domain were reintroduced by complete reflection of the particle trajectory. Particles that exited the domain horizontally ($x_p < 0$) were removed permanently.

The model was implemented twice, once using the results from the salinity minimum simulation and once using the results from the estuarine circulation simulation. Each particle tracking simulation used an initial number of 1,000 particles located uniformly in a vertical line at y = 20 km and released at slack before ebb. The tracking algorithm continued until all particles left the domain at y = 0 km (mouth).

Sediment transport model

The results of the hydrodynamic model also were used for numerical simulations of cohesive sediment transport using the 3D finite element model RMA11 (King, 1996). Current velocities and depth results from the hydrodynamic model were used as input for solution of the advection diffusion constituent transport equation. Initial bed mass was a uniformly distributed layer 0.003 m thick. Surface erosion was calculated with

$$E_s = M \frac{\tau_b - \tau_{ce}}{\tau_{ce}} \quad \text{when } \tau_b > \tau_{ce}$$

(18)

where τ_{ce} is the critical shear stress for erosion and M is the bed erodibility constant, set at 0.02 Nm^{-2} and 0.002 kgm^{-2}s^{-1}, respectively. For the case of a rough bed the bed shear stress, τ_b, is proportional to the shear velocity squared ($\tau_b = \rho \, u_*^2$) determined from

$$u_* = \frac{v_k \, v}{\ln(12.27 \, d/r)}$$

(19)

where r is the roughness height (set to 0.005 m), d is the depth, v_k is von Karman's constant (0.4), and v is the near bed velocity. Deposition was allowed to occur for near-bed shear stress values less than 0.02 Nm^{-2} with a settling velocity of 0.002 ms^{-1}.

RESULTS AND DISCUSSION

The results for the four types of numerical simulations that were done demonstrate the establishment and the effects of the salinity minimum. The simulations using the 1D finite difference model clearly demonstrate the creation of a local salinity minimum. The simulations using the 3D finite element model illustrate the tidally averaged velocity fields resulting from the two distinctive longitudinal density gradient structures—one that contains a local minimum and one having a constant direction gradient. The particle tracking model is used to quantify the increased residence time due to

the circulation associated with the salinity minimum when compared to the circulation associated with the constant direction gradient. The simulations using the sediment transport model demonstrate the increased near-bed convergence of the salinity minimum.

Creation of salinity minimum (results from the 1D finite difference model)

The results from the 1D finite difference model confirm that the observed salinity minimum in Mare Island Strait is created by the phasing of the currents at the junction of Mare Island and Carquinez Straits. Figure 4a displays the time series of measured salinity from the lower sensor at site Car used as the open-end boundary condition in the model. Figure 4b shows model time series of velocity at the mouth of the channel. The vertical shaded region shows the relation between a representative flood current and the boundary receiving first a decreasing and then an increasing salinity. Comparison of the results from the model and measured data for site MIC (Figure 4c) shows that this simple model is accurately predicting the main features of the measured time series of salinity in Mare Island Strait. The shaded region shows a decreasing
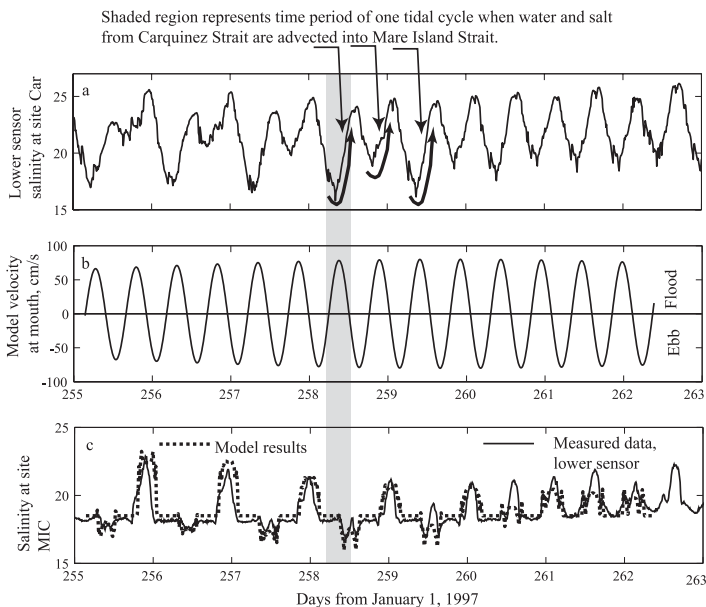
Figure 4. Time series of salinity from field data and 1D difference model results. (a) site Car field data used as boundary condition, including all constituents; (b) model velocity at mouth; (c) site MIC field data and model results.
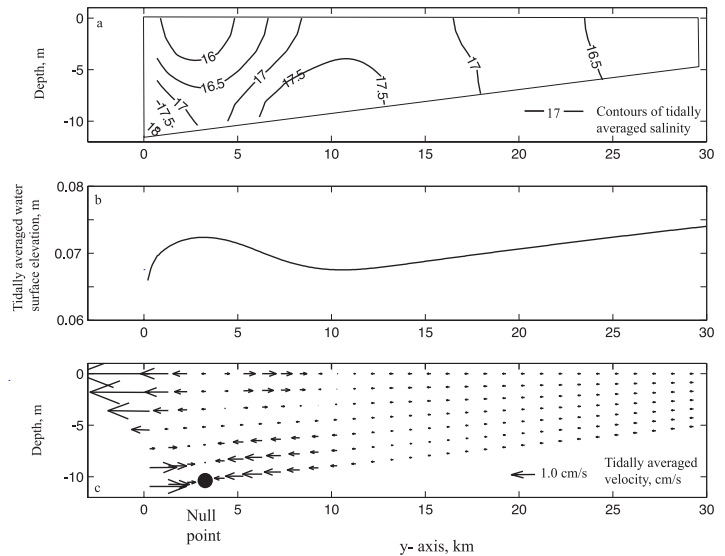
Figure 5. Salinity minimum 3D model results showing tidally averaged values of (a) salinity; (b) water surface elevation; (c) horizontal velocities. Every tenth longitudinal node and every other vertical node is shown for clarity.

and an increasing salinity (the salinity minimum) during the flood current. These model results confirm that the phasing of the currents at the junction of the two straits is responsible for the development of the local salinity minimum in Mare Island Strait.

Residual circulation patterns (finite element model)

Simulations using the 3D finite element model characterize the tidally averaged current structures in the y–z plane that are referred to as the salinity minimum and the constant direction gradient circulation patterns. Current phasing at the junction develops a tidally averaged local salinity minimum centered near y = 3 km (Figure 5a), creating opposing baroclinic pressure gradients. Figure 5b shows the profile of tidally averaged water surface elevation associated with the converging baroclinic gradients. Increased water level occurs from y = 0 to y = 10 km, and two locations of zero water surface slope occur at 3 and 10 km. The salinity minimum circulation (Figure 5c) consists of near-bed velocities that converge from either side of the salinity minimum to meet at a null point that develops near y = 3km. Magnitudes of the modeled velocities are comparable to the observed tidally averaged velocities at sites M5 and M14. Diverging surface currents are required to satisfy continuity.
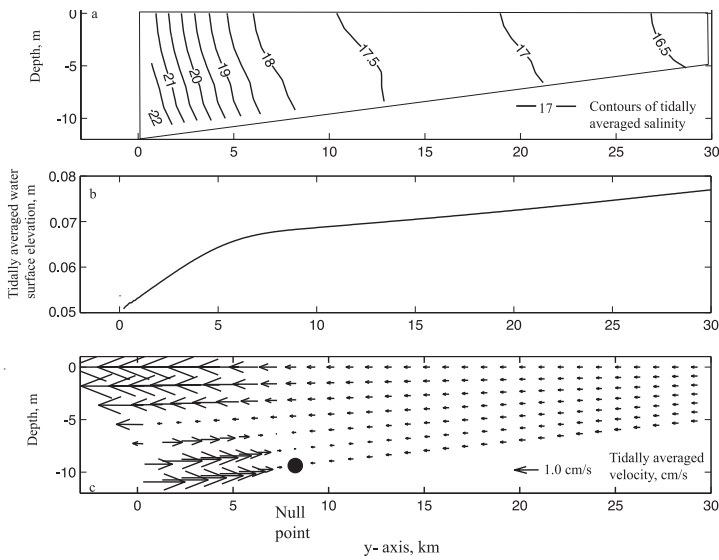
Figure 6. Constant direction gradient 3D model results showing tidally averaged values of (a) salinity; (b) water surface elevation; (c) horizontal velocities. Every tenth longitudinal node and every other vertical node is shown for clarity.

The constant direction longitudinal density gradient results (Figure 6a) show a 0.5 km^{-1} tidally averaged salinity gradient between y = 0 and 8 km representative of the boundary condition applied. Tidally averaged water surface elevation increases in this part of the channel as the barotropic gradient responds to the baroclinic gradient (Figure 6b). Beyond this distance the water surface gradually increases along the remaining length of the channel, indicative of the low inflow at the upstream boundary. At the mouth the baroclinic pressure gradient is -2x10^{-6} m/m, slightly greater than the barotropic pressure gradient, creating a circulation in which tidally averaged currents near the bed are directed upstream (Figure 6c). Near channel kilometer 8 the two pressure gradients are equal at the bed, and the near-bed null point is established. Near the free surface the tidally averaged currents are in the downstream direction. Near the mouth the surface currents are larger than further up the channel to compensate for the upstream near-bed currents because continuity requires that the net flow across a vertical plane be constant along the length of the channel. Upstream of the null point, the baroclinic pressure gradient is weaker than the barotropic pressure gradient throughout the water column, resulting in downstream flow throughout the depth of the channel.

Effects on residence time (particle tracking)

The results from the particle tracking model quantify how the salinity minimum and the constant direction gradient circulation patterns affect residence times in the y-z plane. Figure 7 shows the number of particles remaining in the system over time. More neutrally buoyant particles remained in the domain longer when the circulation was affected by salinity minimum than when the circulation developed from the constant direction gradient. The median residence time of the particles is 169 days for the salinity minimum and 139 days for the constant direction gradient. This represents at least a 30% increase in residence time due to the circulation caused by the salinity minimum.

The near-bed null point for the salinity minimum simulation was located near channel kilometer 3 and for the constant direction gradient circulation near channel kilometer 8. The converging flow near the bed at channel kilometer 3 in Mare Island Strait seems to explain the spatial distribution of selenium contamination in clams in the Strait. Linville et al. (2002) found that the invasive clam Potomocorbula amurensis bioaccumulates selenium and that selenium concentrations in clams increased as residence time increased. In October 1995, selenium concentrations in clams in Mare Island Strait were greatest near channel
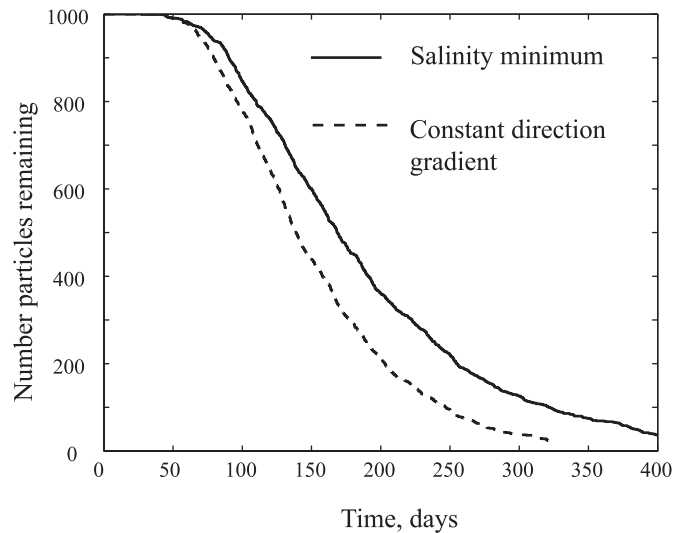

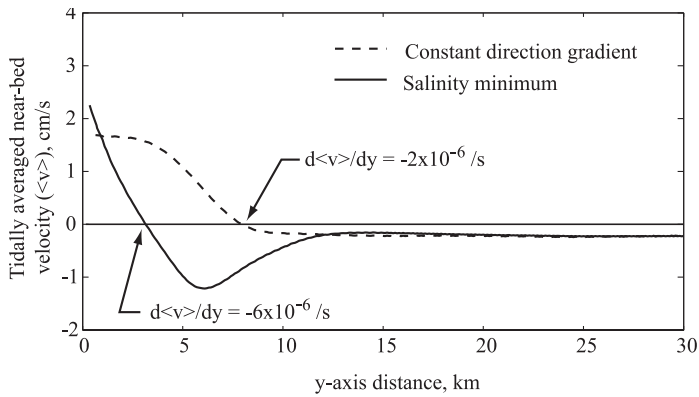Figure 7. Comparison of neutrally buoyant particle residence times.

Figure 8. Convergence rate comparison.

kilometer 3 and smaller landward and seaward (Linville et al. 2002, table 1, Napa channel marker 2). The location of these increased concentrations are consistent with our modeled near-bed null point. The source of selenium was primarily refineries located in Carquinez Strait and Suisun Bay, so convergent transport and not a local source must be responsible for the clam selenium maximum in Mare Island Strait.

A measure of the rate at which the tidally averaged velocities converge towards the null point can be obtained by calculating the rate of change of the tidally averaged velocity along the bottom with respect to distance (Figure 8). The convergence rates are approximately -3×10^{-6} s^{-1} for the salinity minimum and approximately -1×10^{-6} s^{-1} for the constant direction gradient.

This increased convergence is confirmed by the results from the sediment transport simulations (Figure 9). After four tidal cycles, the simulation from the salinity minimum shows a strong depositional feature near the null point at y = 3km. The constant direction gradient simulation shows slightly greater deposition only at the y = 8 km null point. These model results emphasize that (1) the salinity minimum circulation will create a greater deposition of sediment than the constant direction gradient circulation will, and (2) the null point and depositional location will be closer to the mouth of the channel for the salinity minimum circulation than for the constant direction gradient circulation. Mare Island Strait has historically shown increased deposition rates and at one time represented almost half of the total volume of U.S. Army Corps

maintenance dredging in San Francisco Bay (U.S. Army Corps of Engineers 1975).

SUMMARY

Residence times of dissolved substances and sedimentation rates in tidal channels are influenced by residual circulation patterns. One influence on the circulation pattern is the longitudinal density gradient. Typically an estuary has a longitudinal density gradient that maintains the same sign but varies in strength along the length of the estuary. The change in magnitude of the density gradient will cause convergent or divergent circulation patterns that create regions of deposition and erosion. Channel junctions can alter not only the magnitude but also the direction of the longitudinal density gradient and produce a local salinity (density) minimum.

This paper demonstrated and discussed the effects associated with a salinity minimum by applying four numerical models. (1) A simple one-dimensional finite difference model demonstrated that a local salinity minimum is advected into Mare Island Strait from the
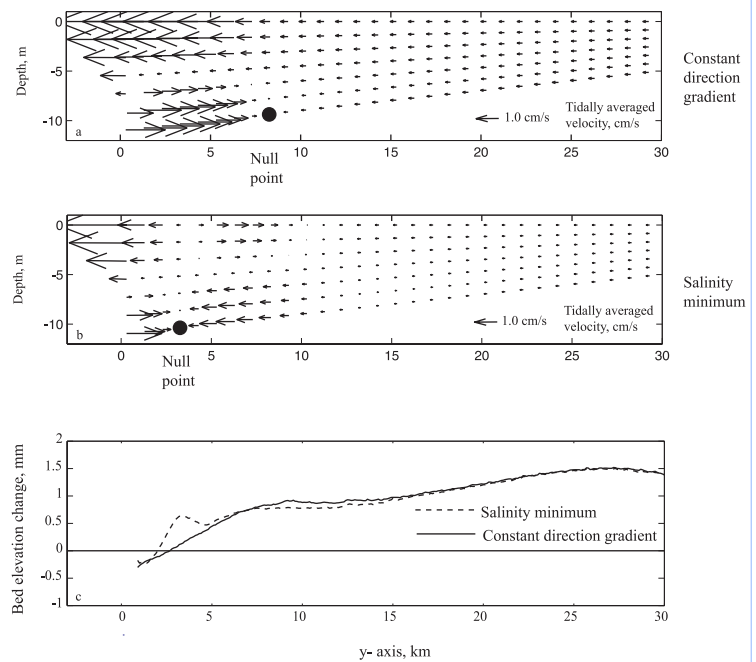

Figure 9. Depositional pattern along y-axis channel after four tidal cycles for the salinity minimum and constant direction gradient simulations.

junction during flood tide. (2) Results from a three-dimensional hydrodynamic finite element model show that a tidally averaged salinity minimum circulation is characterized by converging flow at the bed and diverging flow at the surface, differing from a constant direction gradient circulation having converging flow at the bed and downstream surface currents. The velocity fields are used to drive both a particle tracking and a sediment transport model. (3) A particle tracking model demonstrates a 30 percent increased residence time of neutrally buoyant particles transported through the salinity minimum circulation, as compared to transport through a constant direction gradient circulation. (4) A sediment transport model demonstrates enhanced deposition at the null point of the salinity minimum circulation, as compared to the constant direction gradient circulation. The model simulations are consistent with forcings during dry season periods and these conditions occur the majority of the time in the Napa River. The model results are corroborated by historically noted large sedimentation rates and a local maximum of selenium accumulation in clams at the null point in Mare Island Strait.

ACKNOWLEDGMENTS

REFERENCES

Burau, J.R., Gartner, J.W., and Stacey, M. 1998. Results from the Hydrodynamic Element of the 1994 Entrapment Zone Study in Suisun Bay, in Report of the 1994 Entrapment Zone Study, Wim Kimmerer, Ed., Technical Report 56, Interagency Ecological Program for the San Francisco Bay/Delta Estuary.

Bogle, G. 1997. Stream velocity profiles and longitudinal dispersion. Journal of Hydraulic Engineering 123, No. 9:816-820.

Cook, C.B. 2000. Internal Dynamics of a Terminal Basin Lake: A Numerical Model for the Management of the Salton Sea. Ph.D. Dissertation. Department of Civil and Environmental Engineering, University of California, Davis.

Dimou, K.N., and Adams, E.E. 1993. A random-walk, particle tracking model for well-mixed estuaries and coastal waters. Estuarine, Coastal, and Shelf Science 37:99-110.

Dunsbergen, D.W., and Stelling, G.S. 1993. A 3D particle model for transport problems in transformed coordinates." Delft University of Technology, Department of Civil Engineering, Hydraulic and Geotechnical Engineering Division, Hydromechanics Group, Report No. 93-7.

Fischer, H.B., List, E.J., Koh, R.C.Y., Imberger, J., and Brooks, N.H. 1979. Mixing in Inland and Coastal Waters. Academic Press, New York.

Hansen, D.V., and Rattray, M., Jr. 1965. Gravitational circulation in straits and estuaries. Journal of Marine Research 23:104-122.

Henderson-Sellers, B. 1982. A simple formula for vertical eddy diffusion coefficients under conditions of nonneutral stability. Journal of Geophysical Research 87, No. C8: 5860-5864.

Ippen, A.T. 1966. Estuary and Coastline Hydrodynamics. McGraw-Hill Book Company, Inc., New York.

Jay, D.A., and Musiak, J.D. 1994. Particle trapping in estuarine tidal flows. Journal of Geophysical Research 99, No. C10:20445-20461.

King, I. P. 1996. Program Documentation, RMA-11 – A three dimensional finite element model for water quality in estuaries and streams. University of California, Davis.Largier, J.L., Hearn, C.J., and Chadwick, D.B. 1996. Density structures in "Low Inflow Estuaries." Coastal and Estuarine Studies: Buoyancy Effects on Coastal and Estuarine Dynamics. Edited by Aubrey and Friedrichs, American Geophysical Union. p. 227-241.

Linville, R.G., Luoma, S.N., Cutter, L., and Cutter, G.A. 2002. Increased selenium threat as a result of invasion of the exotic bivalve Potamocurbula amurensis into the San Francisco Bay-Delta. Aquatic Toxicology 57, No. 1-2:51-64.

Mellor, G.L., and Yamada, T. 1982. Development of turbulence closure model for geophysical fluid problems. Reviews of Geophysics and Space Physics 20, No. 4:851-875.

Pollock, D.W. 1994. User's Guide for MODPATH/MOD-PATH-PLOT, Version 3: A particle tracking post-processing package for MODFLOW, the U.S. Geological Survey finite-difference ground-water flow model. U.S. Geological Survey Open-File Report 94-464. Reston, Virginia.

Smith, P.E. 1997. A Three-Dimensional, Finite Difference Model for Estuarine Circulation." Ph. D. Dissertation, Department of Civil and Environmental Engineering, University of California, Davis.

U.S. Army Corps of Engineers. 1975. Final Composite Environmental Statement, Maintenance Dredging, Existing Navigation Projects, San Francisco Bay Region, California. Volume I. San Francisco District.

Warner, J.C., Schoellhamer, D.H., Burau, J.R., and Schladow, S.G. 2002. Effects of tidal current phase at the junction of two straits. Continental Shelf Research 22:1629-1642.

Warner, J.C. 2000. Barotropic and baroclinic convergence zones in tidal channels. Ph.D. Dissertation, Department of Civil and Environmental Engineering, University of California, Davis.

Warner, J.C., Schladow, S.G., and Schoellhamer, D. H. 1999. Summary and Analysis Hydrodynamics and Water-Quality Data for the Napa/Sonoma Marsh Complex, Final Report, Equipment Deployment from September 1997 to March 1998. University of California, Davis, Environmental Dynamics Laboratory Report No. 98-07.

Wolanski, E. 1988. Circulation anomalies in tropical Australian Estuaries. Hydrodynamics of Estuaries, Volume II. Estuarine Case Studies. Edited by Bjorn Kjerfve. CRC Press, Inc. p. 53-59.